SUPPORTING INFORMATION FOR:

Solution NMR structure, backbone dynamics, and heme-binding properties of a novel cytochrome *c* maturation protein CcmE from *Desulfovibrio vulgaris*.

James M. Aramini,[*,†,⊥] Keith Hamilton,[†,⊥] Paolo Rossi,[†,⊥] Asli Ertekin,[†,⊥] Hsiau-Wei Lee,[⊥,‡] Alexander Lemak,[⊥,§] Huang Wang,[†,⊥] Rong Xiao,[†,⊥] Thomas B. Acton,[†,⊥] John K. Everett,[†,⊥] and Gaetano T. Montelione[*,†,⊥,||]

[†] *Center for Advanced Biotechnology and Medicine, Department of Molecular Biology and Biochemistry, Rutgers, The State University of New Jersey, Piscataway, New Jersey 08854, United States*

[‡] *Complex Carbohydrate Research Center, The University of Georgia, Athens, Georgia 30602, United States*

[§] *Ontario Cancer Institute, Department of Medical Biophysics, University of Toronto, Toronto, Ontario, Canada M5G 1L7*

[||] *Department of Biochemistry, Robert Wood Johnson Medical School, University of Medicine and Dentistry of New Jersey, Piscataway, New Jersey 08854, United States*

[⊥] *Northeast Structural Genomics Consortium*

Materials and Methods

Preparation of dvCcmE´Δ9. An 85-residue construct from the *ccmE* gene of *Desulfovibrio vulgaris* strain Hildenborough corresponding to residues 44 to 128 in the wild type protein (UniProtKB/TrEMBL ID, Q72D78_DESVH; NESG ID, DvR115G; hereafter referred to as dvCcmE´Δ9) was cloned into pET21_NESG vector containing an N-terminal methionine and C-terminal affinity tag (LEHHHHHH) to yield the plasmid DvR115G-21.2. The truncated dvCcmE´Δ9 sequence was designed on the basis of secondary structure and disorder prediction methods (*1*). The DvR115G-21.2 plasmid was transformed into codon enhanced BL21 (DE3) pMGK *Escherichia coli* cells, and cultured in MJ9 minimal medium (*2*) containing $(^{15}NH_4)_2SO_4$ and *U*-^{13}C-glucose as the sole nitrogen and carbon sources. Initial cell growth was carried out at 37^{o}C and protein expression was induced at 17^{o}C by isopropyl-β-D-thiogalactopyranoside (IPTG) at mid-log phase growth. Expressed proteins were purified using an ÄKTAxpress™ (GE Healthcare) two-step protocol consisting of HisTrap HP affinity chromatography followed directly by HiLoad 26/60 Superdex 75 gel filtration chromatography. The final yield of purified isotopically-enriched dvCcmE´Δ9 was approximately 28 mg/L of culture. Samples of [*U*-^{13}C,^{15}N]- and [*U*-5%-^{13}C,100%-^{15}N]-dvCcmE´Δ9 for NMR spectroscopy were concentrated by ultracentrifugation to 0.6 to 1.3 mM in 90% H_2O / 10% $^{2}H_2O$ solution containing 20 mM ammonium acetate, 200 mM NaCl, 10 mM DTT, 5 mM $CaCl_2$ at pH 4.5. Sample purity and molecular mass were confirmed by SDS-PAGE and MALDI-TOF mass spectrometry (MALDI-TOF mass of [*U*-^{13}C,^{15}N]-dvCcmE´Δ9 (Da): experimental, 10,792; expected, 10,950). Analytical gel filtration chromatography, static light scattering and ^{15}N T_1 and T_2 relaxation data demonstrate that the protein is monomeric in solution under the conditions used in the NMR studies.

Preparation of dvCcmE′, [C127A]-dvCcmE′, and [Y131F]-dvCcmE′. To probe the dynamics and heme-binding properties of dvCcmE, we cloned, expressed, and purified a redesigned, tagless version of the protein containing the complete C-terminus. A 94-residue construct from the *ccmE* gene of *Desulfovibrio vulgaris* strain Hildenborough corresponding to residues 44 to 137 in the wild type protein (UniProtKB/TrEMBL ID, Q72D78_DESVH; NESG ID, DvR115; hereafter referred to as dvCcmE′) was cloned into pET15TEV_NESG vector containing an N-terminal hexa-His purification tag and TEV protease cleavage site (MGHHHHHHENLYFQSHM) to yield the plasmid DvR115-44-137-14.3. This design results in an additional three N-terminal residues (SHM) after TEV cleavage. In order to minimize the potential of spurious interactions with heme in the *in vitro* heme-binding experiments, the non-native histidine introduced in the initial construct design was mutated to an alanine (QuikChange, Stratagene), resulting in a dvCcmE′ protein comprising residues 44 to 137 of the native sequence preceded by an additional three residues (SAM) at the N-terminus. Isotopically-enriched samples of dvCcmE′ were expressed in BL21 (DE3) pMGK *E. coli* cells cultured in MJ9 minimal medium (*2*) containing $(^{15}NH_4)_2SO_4$ and *U*-^{13}C-glucose as the sole nitrogen and carbon sources, as described above, and initially purified using an ÄKTAxpress™ (GE Healthcare) two-step protocol consisting of a HisTrap HP affinity column followed directly by HiLoad 26/60 Superdex 75 gel filtration column. The resulting fusion protein was then cleaved by incubation with 1 mg N-terminal hexa-His tagged TEV protease (*3*) overnight at 4^{o}C in pH 6.5 buffer containing 20 mM MES, 100 mM NaCl, 10 mM DTT, and 5 mM $CaCl_2$. After incubation with TEV protease, the mixture was passed over 2 ml Ni-NTA Superflow resin (Qiagen) to remove the cleaved hexa-His tag and TEV protease, followed by a final gel filtration purification step on a HiLoad 26/60 Superdex 75 column. The final yield of purified isotopically-enriched dvCcmE′ was approximately 45 mg/L of culture. A sample of [*U*-

$^{13}C,^{15}N$]-dvCcmE′ for NMR spectroscopy was concentrated by ultracentrifugation to 1.1 mM in 90% H_2O / 10% ^2H_2O solution containing 20 mM MES, 100 mM NaCl, 10 mM DTT, 5 mM $CaCl_2$ at pH 6.5. Sample purity and molecular mass were confirmed by SDS-PAGE and MALDI-TOF mass spectrometry. Single residue mutations of dvCcmE′, [C127A]-dvCcmE′ and [Y131F]-dvCcmE′, were cloned using the QuikChange site-directed mutagenesis kit (Stratagene), and expressed and purified as described above for wild type dvCcmE′. All of the expression plasmids used in this work are available from the PSI Materials Repository (http://psimr.asu.edu/).

NMR Spectroscopic Studies of dvCcmE′Δ9. All NMR data on samples of dvCcmE′Δ9 were collected at 25°C on Varian INOVA 600 MHz and Bruker AVANCE 600 and 800 NMR spectrometers equipped with 5 mm TXI cryoprobes, processed with NMRPipe (*4*), and visualized using SPARKY (*5*). All spectra were referenced to internal DSS. Complete ^1H, ^{13}C, and ^{15}N resonance assignments for dvCcmE′Δ9 were determined using conventional triple resonance NMR methods. Backbone resonance assignments were made by combined use of AutoAssign 2.4.0 (*6*) and PINE 1.0 server (*7*) using peak lists from 2D ^1H-^{15}N HSQC and 3D HNCO, HN(CA)CO, HN(CO)CA, HNCA, CBCA(CO)NH and HNCACB spectra. Side chain assignment was completed manually using 3D HBHA(CACO)NH, HCCH-COSY, HCCH-TOCSY and (H)CCH-TOCSY experiments. Stereospecific isopropyl methyl assignments for all Val and Leu residues were deduced from characteristic cross-peak fine structures in high resolution 2D ^1H-^{13}C HSQC spectra of [*U*-5%-^{13}C,100%-^{15}N]-dvCcmE′Δ9 (*8*). Resonance assignments were validated using the Assignment Validation Suite (AVS) software package (*9*). Three-bond $^3J(H^N\text{-}H^\alpha)$ scalar couplings were determined using the 3D HNHA experiment (*10*). ^1H-^{15}N heteronuclear NOE and ^{15}N T_1 and T_2 relaxation measurements were made using gradient sensitivity-enhanced 2D heteronuclear NOE and 1D ^{15}N T_1 and T_2 (CPMG) relaxation

experiments, respectively (*11*). One-bond ^{15}N-^{1}H residual dipolar couplings (RDCs), $^{1}D_{NH}$, were obtained on [*U*-5%-^{13}C,100%-^{15}N]-dvCcmE′Δ9 aligned in 4.2% C12E5 (PEG, Sigma Aldrich) using standard protocols (*12*). The RDCs were determined from $^{1}J(H^{N}$-N) scalar couplings measured from an interleaved pair of 2D ^{1}H-^{15}N TROSY-HSQC acquisitions on isotropic and aligned samples (*13*). Final chemical shift assignments, NOESY peak lists, time domain data, and RDC data for dvCcmE′Δ9, as well as backbone assignments, relaxation data, and time domain data for dvCcmE′ (described below) were deposited into the BioMagResDB (BMRB accession numbers, 16096 and 18380, respectively).

Solution Structure Determination of dvCcmE′Δ9. The solution NMR structure of dvCcmE′Δ9 was calculated using CYANA 3.0 (*14,15*) supplied with peak intensities from 3D simultaneous CN NOESY (*16*) (τ_m = 100 ms) and 3D ^{13}C-edited aromatic NOESY (τ_m = 120 ms) spectra, together with broad dihedral angle constraints ($\phi \pm 30°$; $\psi \pm 30°$) computed by TALOS (*17*) for ordered residues with confidence scores of 10, and 49 $^{1}D_{NH}$ RDCs for ordered residues from the single alignment medium. The 20 structures with lowest target function out of 100 in the final cycle calculated were further refined by restrained molecular dynamics in explicit water using CNS 1.1 (*18,19*) and the PARAM19 force field, using the final NOE derived distance constraints, TALOS dihedral angle constraints, and $^{1}D_{NH}$ RDCs. The final refined ensemble of 20 structures (excluding the not-well-defined C-terminal hexa-His polypeptide segment) and structure constraints were deposited into the Protein Data Bank (PDB ID, 2KCT). Structural statistics and global structure quality factors, including Verify3D (*20*), ProsaII (*21*), PROCHECK (*22*), and MolProbity (*23,24*) raw and statistical *Z*-scores, were computed using the PSVS 1.4 software package (*25*). The global goodness-of-fit of the final structure ensemble with the NOESY peak list data and RDCs was determined using the RPF analysis (*26*) and PALES (*27*) programs, respectively. Structure-based sequence alignments and coordinate

superimpositions were obtained from the CE combinatorial extension server (*28*). Conserved residue analysis was performed using the ConSurf server (*29*) on aligned sequences of cysteine-containing CcmE variants extracted from the entire CcmE protein domain family (PF03100; Pfam 24.0; 73 out of 750 sequences). All structure figures were made using PyMOL (*30*).

NMR Spectroscopic Studies of dvCcmE′. NMR data on [*U*-^{13}C,^{15}N]-dvCcmE′ were collected at 25^{o}C on a Bruker AVANCE 600 NMR spectrometer equipped with 5 mm TXI or 1.7 mm TCI cryoprobes, processed with NMRPipe (*4*), and visualized using SPARKY (*5*). All spectra were referenced to internal DSS. Backbone ^{1}H, ^{13}C, and ^{15}N resonance assignments for dvCcmE′ were made by using the PINE 1.0 server (*7*) with peak lists from 2D ^{1}H-^{15}N HSQC and 3D HNCO, HN(CA)CO, HN(CO)CA, HNCA, CBCA(CO)NH and HNCACB spectra. ^{1}H-^{15}N heteronuclear NOE and ^{15}N T_1 and T_2 relaxation measurements were made using gradient sensitivity-enhanced 2D heteronuclear NOE and 2D ^{15}N T_1 and T_2 (CPMG) relaxation experiments, respectively, collected as pseudo-3D experiments (*11*). T_1 spectra were acquired with delays, T = 20, 50, 100, 200, 300, 400, 600, 800, 1000, 1200, and 1500 ms, and a relaxation delay of 3 s. T_2 spectra were acquired with CPMG delays, T = 16, 32, 48, 64, 80, 96, 128, 160, 192, 240, and 320 ms, and a relaxation delay of 1.5 s. For the ^{1}H-^{15}N heteronuclear NOE measurements, interleaved NOE on and off experiments were collected with a 3 s proton saturation period and 3 s relaxation delay, respectively.

^{15}N Relaxation Analyses of dvCcmE′. Residue specific ^{15}N longitudinal and transverse relaxation rates (R_1 and R_2) and ^{1}H-^{15}N heteronuclear NOE values were calculated from cross-peak intensities in the respective 2D experiments (*11*) obtained on [*U*-^{13}C,^{15}N]-dvCcmE′ at a ^{15}N Larmor frequency of 60.8 MHz using in-house written codes in MATLAB 7.9.0 (MathWorks). In all cases, peak intensities of resolved resonances were analyzed; data for the handful of severely overlapping resonances were omitted from all analyses. Longitudinal and transverse

relaxation rates were computed by fitting peak intensity $I(T)$ as a function of delay time, T, according to Eqs. 1 and 2, respectively (*31*):

$$I(T) = I_\infty - \left[I_\infty - I_0\right]\exp\{-R_1 T\} \quad (1)$$

$$I(T) = I_0 \exp\{-R_2 T\} \quad (2)$$

The uncertainties of the intensities were estimated from the root-mean-square baseline noise in the spectra. The statistical properties of the resulting relaxation rates were estimated from randomly generated data sets using a Monte Carlo approach, based on the uncertainties of the spectral intensities (*31*). Generalized order parameters, S^2, were computed from the backbone ^{15}N relaxation and ^{1}H-^{15}N heteronuclear NOE data using the ModelFree 4.20 program (*31,32*) interfaced with the FAST-ModelFree program (*33*). An isotropic model for molecular motion was used, yielding an overall rotational correlation time, τ_c, of 6.5 ns.

Heme-Binding Studies of dvCcmE′, [C127A]-dvCcmE′, and [Y131F]-dvCcmE.′ All *in vitro* heme-binding experiments were performed under aerobic conditions, but all buffers were sparged with argon gas immediately prior to use. Because of the well-documented complex speciation of heme in aqueous solution (*34*), we examined many different buffers and conditions for heme binding. We chose buffers containing 5% PEG (polyethylene glycol), which we know from our RDC measurements does not perturb the structure of dvCcmE′, to promote monomeric heme formation. UV-visible absorption spectra were obtained at room temperature on a SpectraMax Plus^{384} UV-visible spectrophotometer (Molecular Devices) equipped with a 96-well microplate. Samples of wild type dvCcmE′ and mutants were made by addition of 0.8 equivalents of freshly prepared hemin ([Fe^{3+}-PPIX]Cl; Sigma) stock solution (0.75 mM in 0.1 N NaOH or DMSO) to 15 μM protein in 50 mM Tris, 100 mM NaCl, 5% PEG, pH 7.5 buffer. Reduced (ferrous) heme forms of each sample were made by microliter addition of freshly

prepared sodium dithionite stock solution (up to 2 mM final). Spectra were acquired simultaneously on each sample over a wavelength range of 250 to 700 nm at 1 nm increments, and corrected by subtraction against a blank well containing buffer only using MATLAB (MathWorks).

Heme stained SDS-PAGE experiments were performed on 16 μg of wild type, [C127A]-, and [Y131F]-dvCcmE′ plus 0.5 equivalents of hemin as well as 1 μg equine heart holocytochrome *c* control (Sigma). Samples of dvCcmE′ were made by addition of 0.5 equivalents of freshly prepared hemin to 15 μl of 0.1 mM protein in 50 mM Tris, 100 mM NaCl, 0.1 mM TCEP, pH 7.5, and incubated in the dark for 15 min. Each protein sample was combined with 5 μl of XT sample buffer (Bio-Rad), boiled for 10 min, and separated by electrophoresis on a NuPAGE 4-12% Bis-Tris gel (Invitrogen) run at 200 V for 35 min in MES SDS running buffer. Heme staining was performed following the protocol of Thomas et al. (*35*), except that half the concentration of TMBZ was used.

Pyridine hemochrome assays were conducted following of Berry and Trumpower (*36*) with minor modifications. Stock solutions of free hemin, wild type dvCcmE′ plus 0.5 equivalents of hemin, [C127A]- dvCcmE′ plus 0.5 equivalents of hemin, and equine heart holocytochrome *c* (Sigma) were diluted in NaOH (50 mM final), followed by addition of pyridine (20% v/v final). In the case of cytochrome *c*, the initial oxidized (ferric) form was made by addition of potassium ferricyanide, $K_3Fe(CN)_6$ (200 μM final). Final concentrations of each sample were as follows: wild type and [C127A]-dvCcmE′, 24 μM; free hemin, 12 μM; cytochrome *c*, 6 μM. UV-visible absorption spectra of each sample were simultaneously acquired at room temperature on a SpectraMax Plus^{384} UV-visible spectrophotometer (Molecular Devices) equipped with a 96-well microplate. Spectra of the oxidized (ferric) forms of each sample were obtained first, followed by *in situ* reduction of each sample by the addition of solid sodium dithionite, and acquisition of

the reduced (ferrous) spectra. The difference UV spectrum (reduced – oxidized) of the α-band region is indicative of covalent binding of heme to a protein. Identical results were obtained for wild type and [C127A]-dvCcmE´ when the proteins were reduced with dithionite prior to addition of the NaOH and pyridine.

Table S1. Summary of NMR and structural statistics for dvCcmE′Δ9[a]

Completeness of resonance assignments[b]	
Backbone (%)	98.6
Side chain (%)	97.2
Aromatic (%)	100
Stereospecific methyl (%)	100
Conformationally-restricting constraints[c]	
Distance constraints	
Total	1384
intra-residue ($i = j$)	344
sequential ($\|i- j\| = 1$)	390
medium range ($1 < \|i – j\| < 5$)	125
long range ($\|i – j\| \geq 5$)	525
distance constraints per residue	15.9
Dihedral angle constraints	79
Hydrogen bond constraints	0
Number of constraints per residue	16.8
Number of long range constraints per residue	6.0
Residual constraint violations[c]	
Average number of distance violations per structure	
0.1 – 0.2 Å	3.6
0.2 – 0.5 Å	0.9
> 0.5 Å	0
average RMS distance violation / constraint (Å)	0.01
maximum distance violation (Å)	0.49
Average number of dihedral angle violations per structure	
1 – 10°	6.3
> 10°	0
average RMS dihedral angle violation / constraint (degree)	0.73
maximum dihedral angle violation (degree)	7.90
RMSD from average coordinates (Å)[c,d]	
backbone atoms	0.5
heavy atoms	0.9
MolProbity Ramachandran statistics[c,d]	
most favored regions (%)	96.3
additional allowed regions (%)	3.5
disallowed regions (%)	0.2

Table S1 (Cont'd). Summary of NMR and structural statistics for dvCcmE′Δ9[a]

Global quality scores [c]		
	Raw	*Z*-score
Verify3D	0.44	-0.32
ProsaII	0.55	-0.41
Procheck(phi-psi) [d]	-0.62	-2.12
Procheck(all) [d]	-0.43	-2.54
MolProbity clash	10.87	-0.34
RPF Scores[e]		
Recall	0.984	
Precision	0.915	
F-measure	0.948	
DP-score	0.795	
RDC Statistics[f]		
Number of $^1D_{NH}$ constraints	49	
R	0.995 ± 0.001	
Q_{rms}	0.096 ± 0.011	

[a] Structural statistics were computed for the ensemble of 20 deposited structures (PDB ID, 2KCT).

[b] Computed using AVS software (*9*) from the expected number of peaks, excluding: highly exchangeable protons (N-terminal and Lys amino and Arg guanido groups, hydroxyls of Ser, Thr, Tyr), carboxyl carbons of Asp and Glu, non-protonated aromatic carbons, and the C-terminal His_6 tag.

[c] Calculated using PSVS 1.4 program (*25*). Average distance violations were calculated using the sum over r^{-6}.

[d] Ordered residue ranges [S(phi) + S(psi) > 1.8]: 52-67,70-79,86-112,115-127.

[e] RPF scores (*26*) reflecting the goodness-of-fit of the final ensemble of structures (including disordered residues) to the NMR data.

[f] Computed from the final ensemble of structures and the residual dipolar coupling data using PALES (*27*).

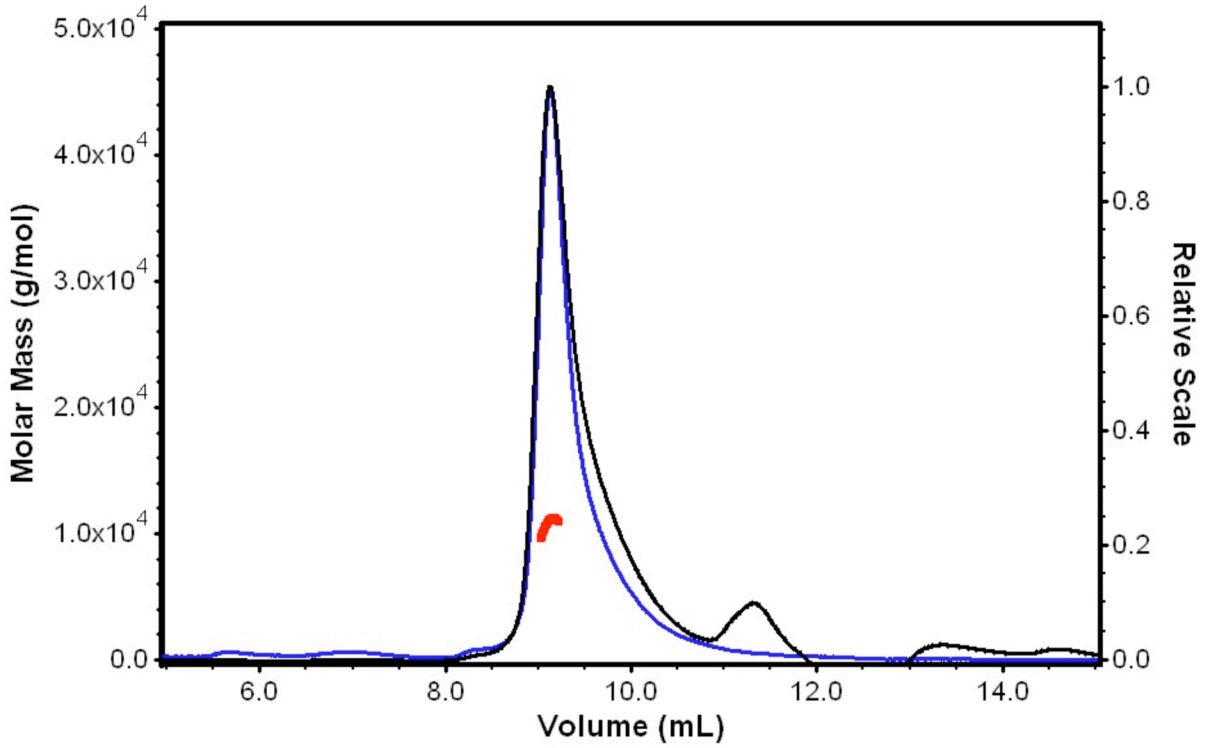

Figure S1. Static light scattering results for dvCcmE´Δ9. Data were collected on a miniDAWN (TREOS) Light Scattering Instrument (Wyatt Technology) at 30°C on an NMR sample (30 µl) of [*U*-^{13}C,^{15}N]-dvCcmE´Δ9 in 20 mM ammonium acetate, 200 mM NaCl, 5 mM $CaCl_2$, 10 mM DTT, 1X Proteinase Inhibitors, 0.02% (w/v) NaN_3, 10% ^2H_2O at pH 4.5. The sample was injected onto an analytical gel filtration column (Protein KW-802.5, Shodex, Japan; flow rate, 0.5 ml/min) with the effluent monitored by refractive index (black trace; Optilab rEX) and 90° static light scattering (blue trace) detectors. The resulting experimental molecular weight of dvCcmE´Δ9 is 10.4 kDa (red); the expected MW including affinity tag is 10.9 kDa.

Figure S2.

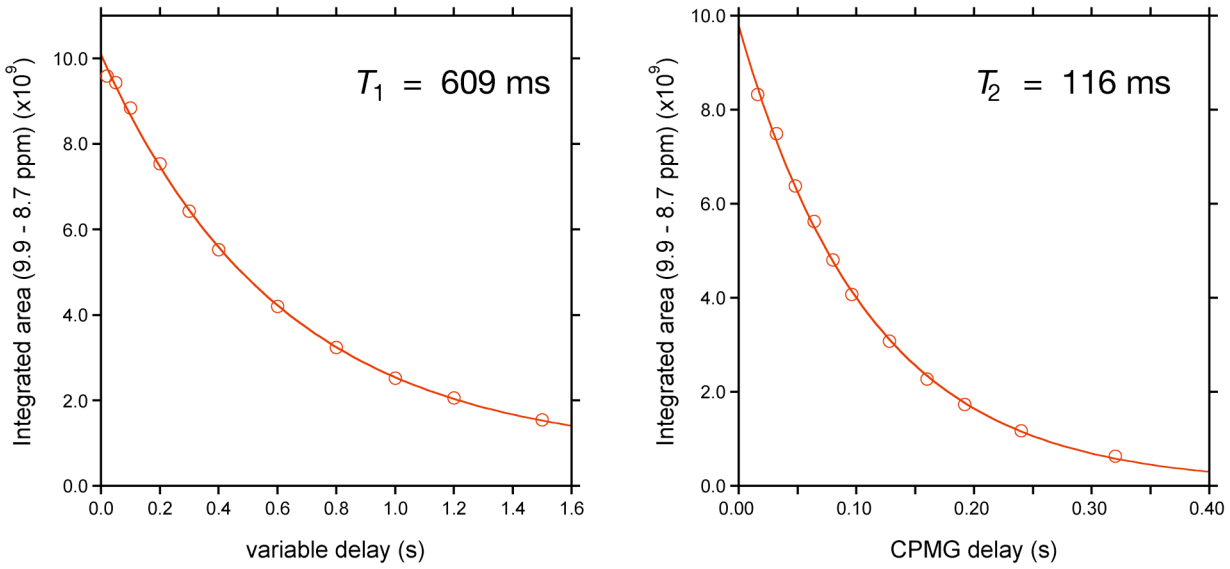
T_1 = 609 ms
Integrated area (9.9 - 8.7 ppm) (x10^9)
variable delay (s)
T_2 = 116 ms
Integrated area (9.9 - 8.7 ppm) (x10^9)
CPMG delay (s)

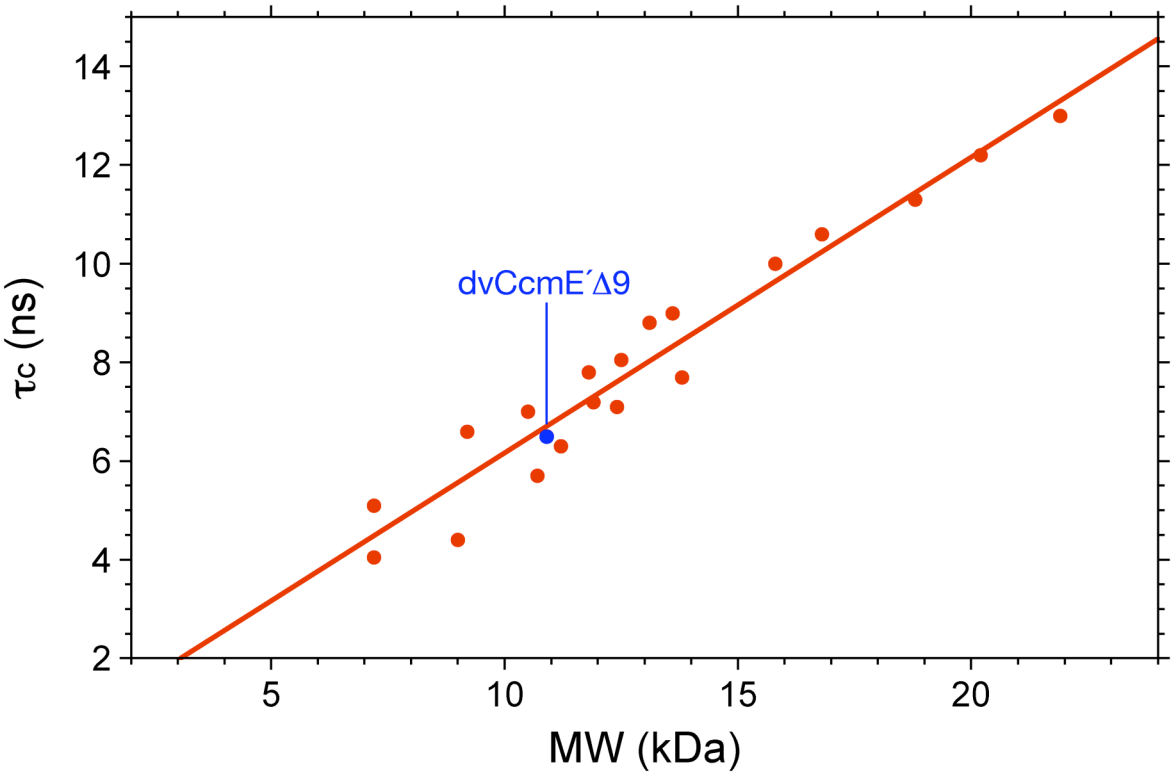
dvCcmE´Δ9
τc (ns)
MW (kDa)

Figure S2. 1D ^{15}N T_1 and T_2 relaxation data for [*U*-^{13}C,^{15}N]-dvCcmE′Δ9. The data were acquired on a Bruker AVANCE 600 MHz spectrometer at 298 K using pseudo-2D ^{15}N T_1 and T_2 gradient experiments (*11*). T_1 spectra were acquired with delays, T = 20, 50, 100, 200, 300, 400, 600, 800, 1000, 1200 and 1500 ms, and a relaxation delay of 3 s. T_2 spectra were acquired with CPMG delays, T = 16, 32, 48, 64, 80, 96, 128, 160, 192, 240, and 320 ms, and with a relaxation delay of 1.5 s. (Top): ^{15}N T_1 and T_2 values were extracted by plotting the decay of integrated $^{1}H^{N}$ intensity between δ ≈ 8.7 to 9.9 ppm and fitting the curves with standard exponential equations using the program 't1guide' within TopSpin 2.1 (Bruker BioSpin). (Bottom): Plot of rotational correlation time, τ_c (ns), versus protein molecular weight (kDa) for known monomeric NESG targets of ranging size (taking into account isotope enrichment as well as affinity tags in the sequence). ^{15}N T_1/T_2 data for all monomeric proteins used for the τ_c vs. MW plot were obtained on the same Bruker 600 MHz spectrometer at 298 K, and analyzed as described above. For each protein, the τ_c was calculated from the ^{15}N T_1/T_2 ratio using the following approximation of literature relaxation equations (*37,38*):

$$\tau_c \approx \left(\sqrt{\frac{6T_1}{T_2} - 7} \right) / 4\pi\nu_N \qquad (3)$$

where ν_N is the resonance frequency of ^{15}N in Hz.

Using this approach, we obtain a τ_c of 6.5 ns for [*U*-^{13}C,^{15}N]-dvCcmE′Δ9, shown in blue, which is consistent with a monomer (expected MW = 10.9 kDa, including the N-terminal Met and C-terminal affinity tag).

Figure S3.

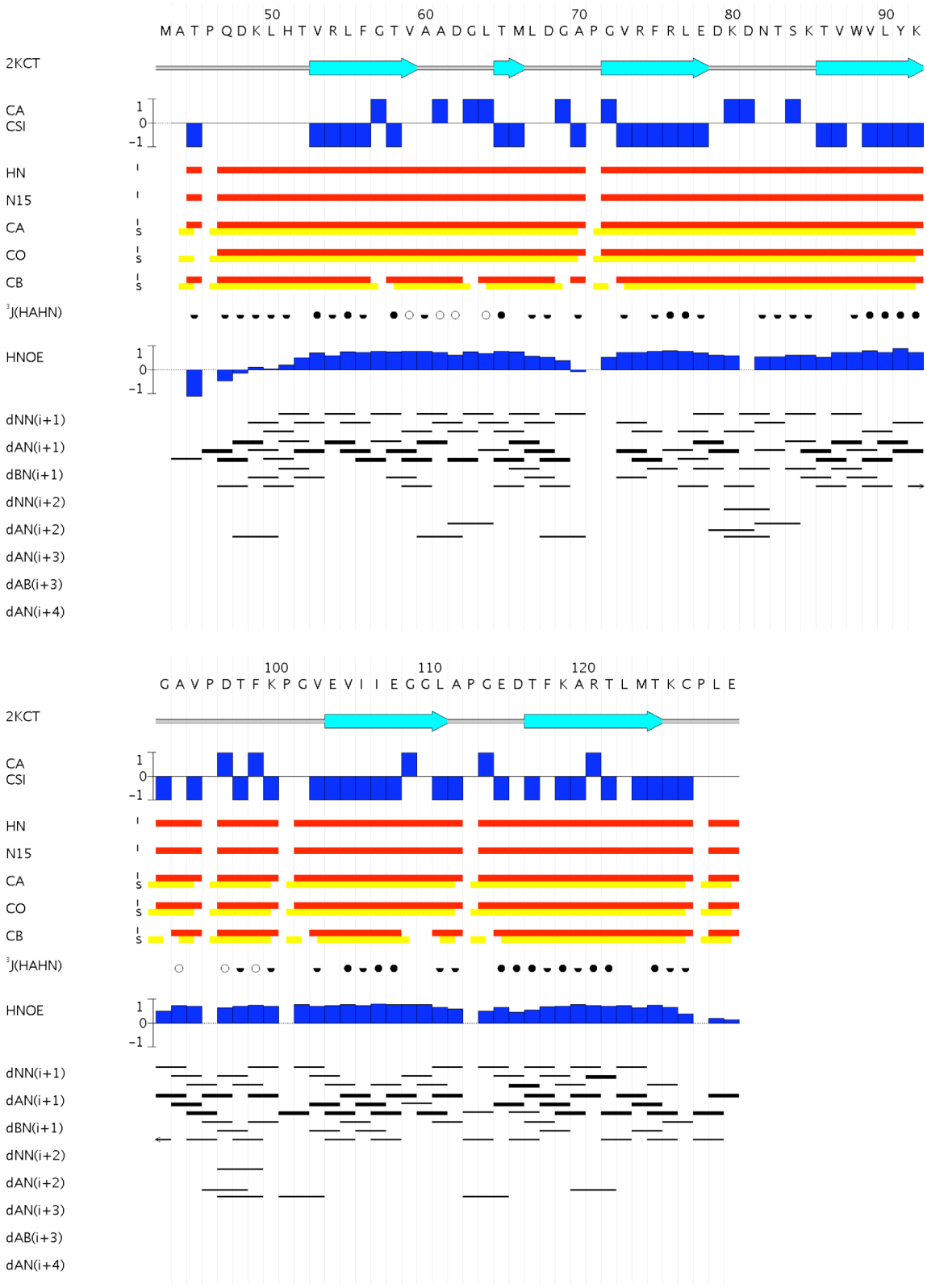
50
60
70
80
90
M A T P Q D K L H T V R L F G T V A A D G L T ML D G A P G V R F R L E D K D N T S K T V WV L Y K
2KCT
CA
CSI
HN
N15
CA
CO
CB
3J(HAHN)
HNOE
dNN(i+1)
dAN(i+1)
dBN(i+1)
dNN(i+2)
dAN(i+2)
dAN(i+3)
dAB(i+3)
dAN(i+4)
100
110
120
G A V P D T F K P G V E V I I E G G L A P G E D T F K A R T L MT K C P L E
2KCT
CA
CSI
HN
N15
CA
CO
CB
3J(HAHN)
HNOE
dNN(i+1)
dAN(i+1)
dBN(i+1)
dNN(i+2)
dAN(i+2)
dAN(i+3)
dAB(i+3)
dAN(i+4)

Figure S3. NMR connectivity map summarizing data used to determine resonance assignments and secondary structure for dvCcmE′Δ9. The final six unassigned histidines in the C-terminal tag have been omitted. Intraresidue (i) and sequential (s) connectivities for the three-rung assignment strategy (*6*) matching intraresidue and sequential C′, C^{α}, and C^{β} resonances are shown as horizontal red and yellow lines, respectively. $^{3}J(H^{N}\text{-}H^{\alpha})$ values range as follows: (o) < 5.0 Hz; (◒) $5.0 \leq J \leq 7.5$ Hz; (●) > 7.5 Hz. Interresidue NOE connectivities are shown as thin, medium, and thick black lines, corresponding to weak, medium, and strong NOE interactions. Bar graphs of CSI (*39*) and $^{1}H\text{-}^{15}N$ heteronuclear NOE data are shown in blue. The secondary structural elements in the final dvCcmE′Δ9 NMR structure (PDB ID, 2KCT) are also shown. In general, the secondary structural elements in the final structure are well-defined by the CSI, $^{3}J(H^{N}\text{-}H^{\alpha})$ scalar coupling and NOESY patterns.

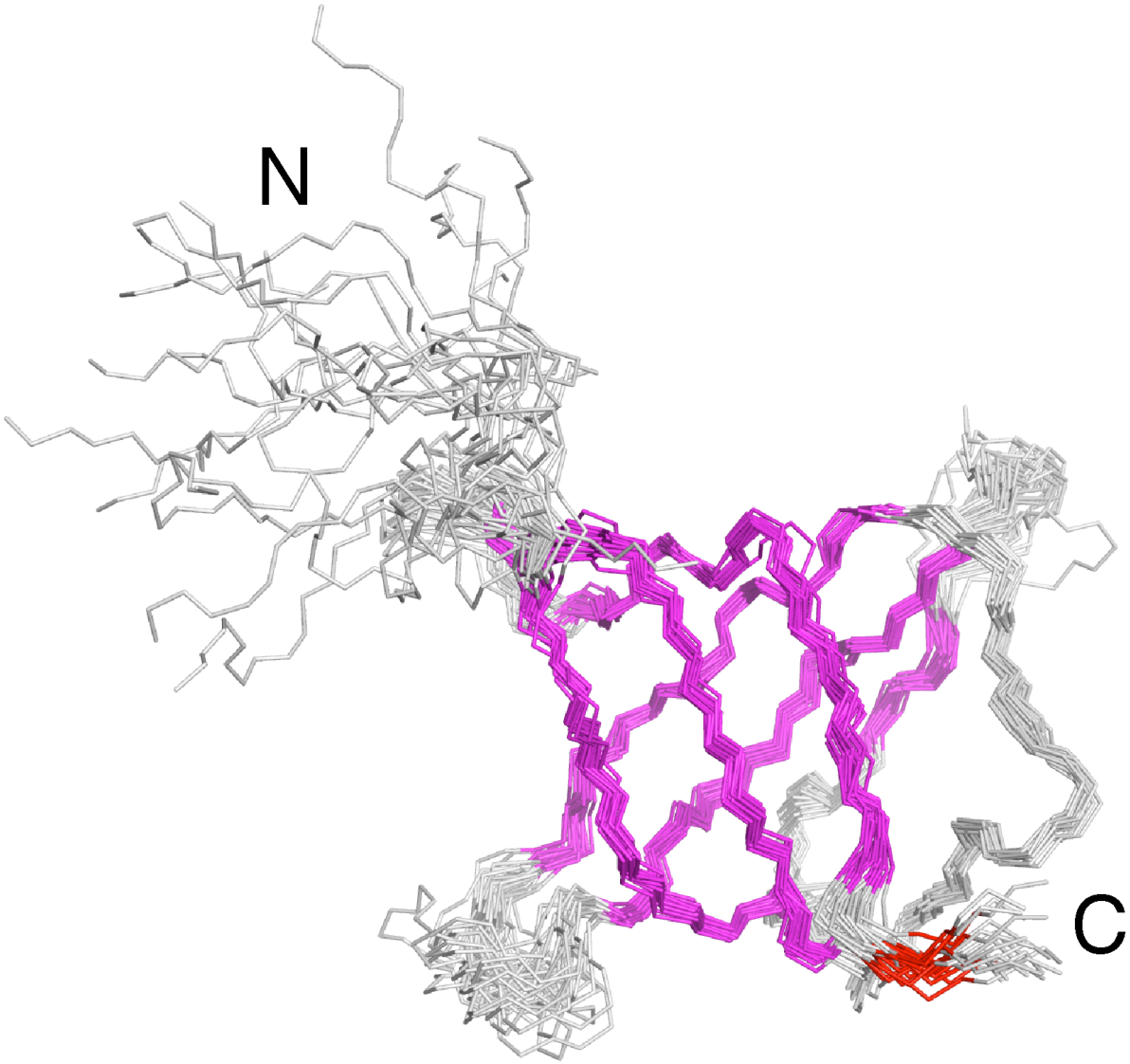

Figure S4. Superposition of the final ensemble of 20 conformers representing the solution NMR structure of apo-dvCcmE′Δ9 (PDB ID, 2KCT); residues 44 to 128 are shown. The β-strands and loops are shown in magenta and grey, respectively. The heme-binding cysteine, C127, is colored red.

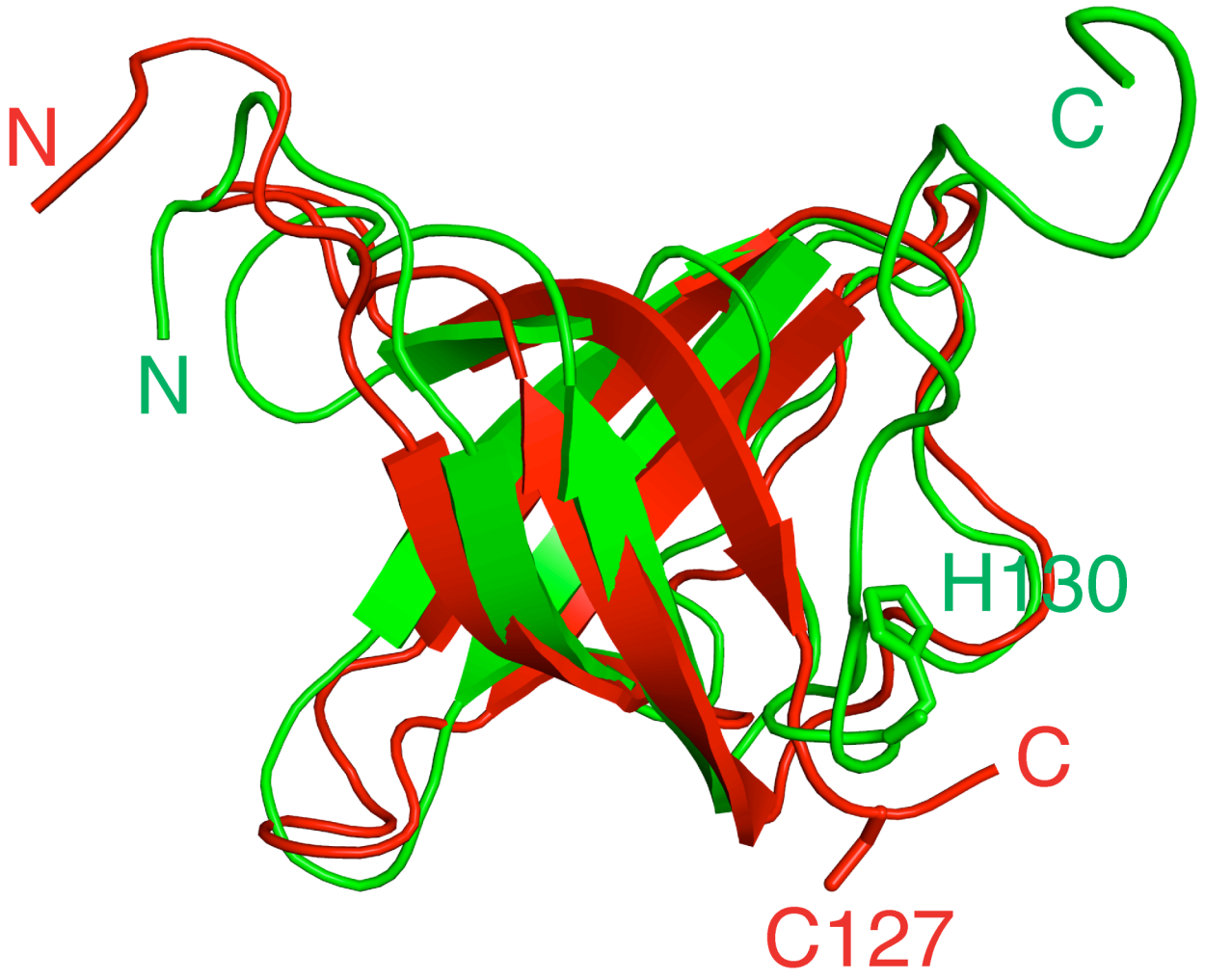

Figure S5. Superposition of the solution NMR structures of dvCcmE′Δ9 (red; residues 47 to 128) and *E. coli* CcmE′ (green, PDB ID, 1SR3; residues 54 to 143) (*40*). Side chains of the heme-binding cysteine (dvCcmE′Δ9) and histidine (ecCcmE′) residues are labeled.

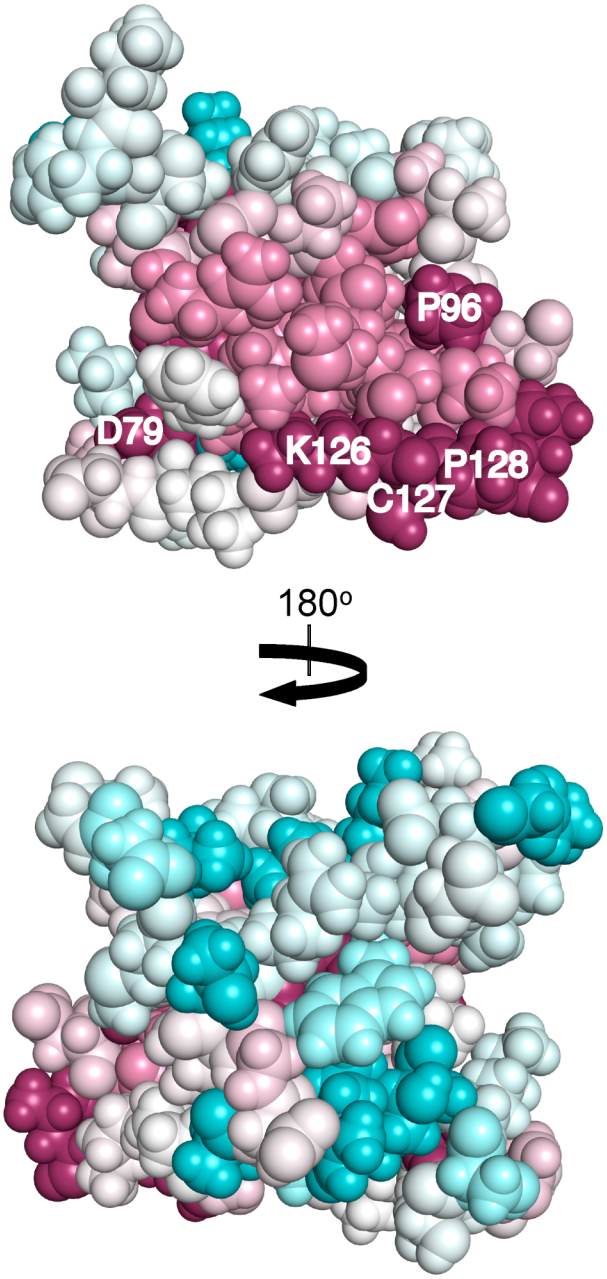

Figure S6. ConSurf (*29*) analysis showing conserved residues on the putative CcmC binding face (top) and opposite face (bottom) of dvCcmE′Δ9 (residues 50 to 128). Residue coloring, reflecting the degree of residue conservation over the variant CcmE sub-family containing a heme-binding cysteine extracted from the entire aligned CcmE protein domain family (PF03100; Pfam 24.0; 73 out of 750 sequences), ranges from magenta (highly conserved) to cyan (variable).

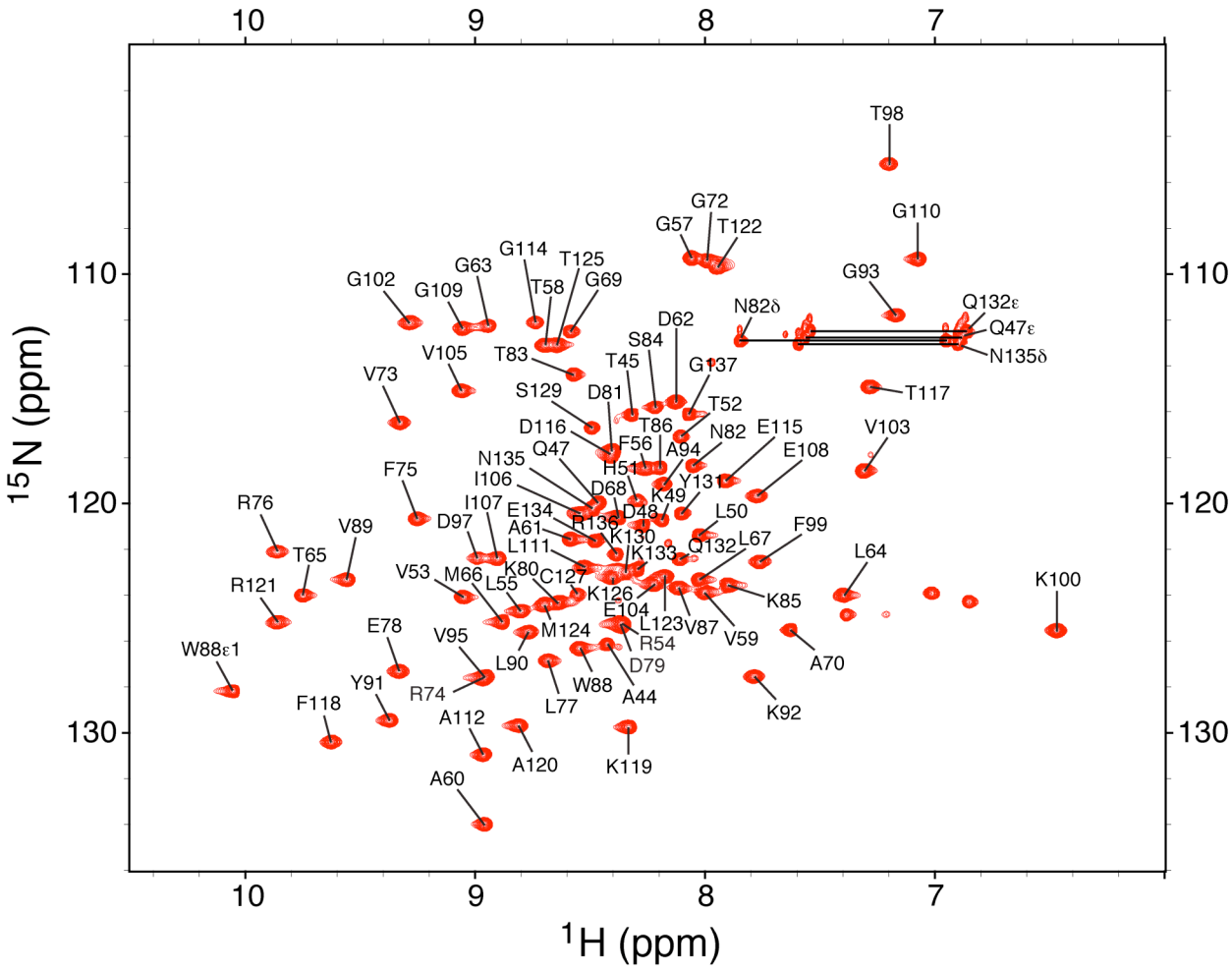

Figure S7. Two dimensional ^{1}H-^{15}N HSQC spectrum of 1.1 mM [*U*-^{13}C,^{15}N]-apo-dvCcmE′ in 90% H_2O / 10% $^{2}H_2O$ solution containing 20 mM MES, 100 mM NaCl, 10 mM DTT, 5 mM $CaCl_2$ at pH 6.5 collected at 25°C on a Bruker AVANCE 600 MHz spectrometer. Backbone resonance assignments are labeled with one-letter amino acid codes followed by their sequence numbers. Assigned side chain NH and NH_2 resonances of Trp, Asn, and Gln are also indicated.

Figure S8.

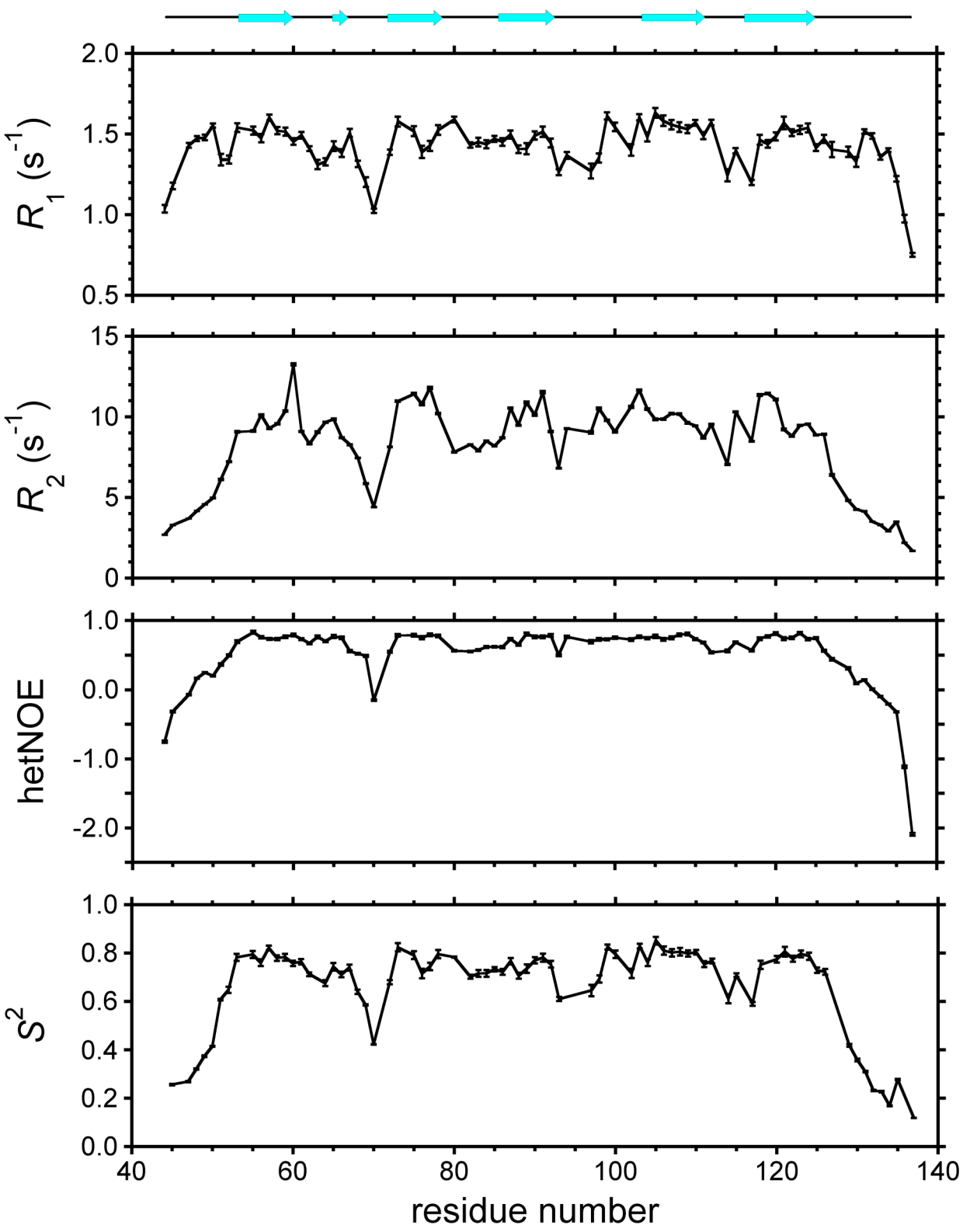
2.0
1.5
1.0
0.5
R_1 (s^{-1})
15
10
5
0
R_2 (s^{-1})
1.0
0.0
-1.0
-2.0
hetNOE
1.0
0.8
0.6
0.4
0.2
0.0
S^2
40
60
80
100
120
140
residue number

Figure S8. Backbone dynamics of apo-dvCcmE′ (residues 44 to 137). Plots of backbone amide ^{15}N relaxation rates, ^{1}H-^{15}N heteronuclear NOEs and generalized order parameters, S^2, versus residue number obtained on [*U*-^{13}C,^{15}N]-dvCcmE′ at pH 6.5 and at a ^{15}N Larmor frequency of 60.8 MHz. Order parameters were computed using the ModelFree 4.20 program (*31,32*) assuming an isotropic model, yielding an overall rotational correlation time, τ_c, of 6.5 ns. Values of ^{15}N R_2/R_1, ^{1}H-^{15}N heteronuclear NOE and S^2 for the C-terminal end of dvCcmE′ are as follows:

Residue	^{15}N R_2/R_1	^{1}H-^{15}N hetNOE (Stnd. Dev.)	S^2 (Stnd. Dev.)
K126	6.076	0.565 (0.013)	0.723 (0.012)
C127	4.565	0.440 (0.020)	no solution
P128	N/A	N/A	N/A
S129	3.460	0.308 (0.015)	0.419 (0.006)
K130	3.208	0.092 (0.013)	0.358 (0.006)
Y131	2.731	0.143 (0.009)	0.310 (0.003)
Q132	2.358	0.009 (0.010)	0.232 (0.003)
K133	2.435	-0.098 (0.008)	0.228 (0.003)
E134	2.078	-0.208 (0.008)	0.169 (0.002)
N135	2.860	-0.320 (0.008)	0.278 (0.003)
R136	2.258	-1.116 (0.016)	no solution
G137	2.265	-2.093 (0.018)	0.119 (0.001)

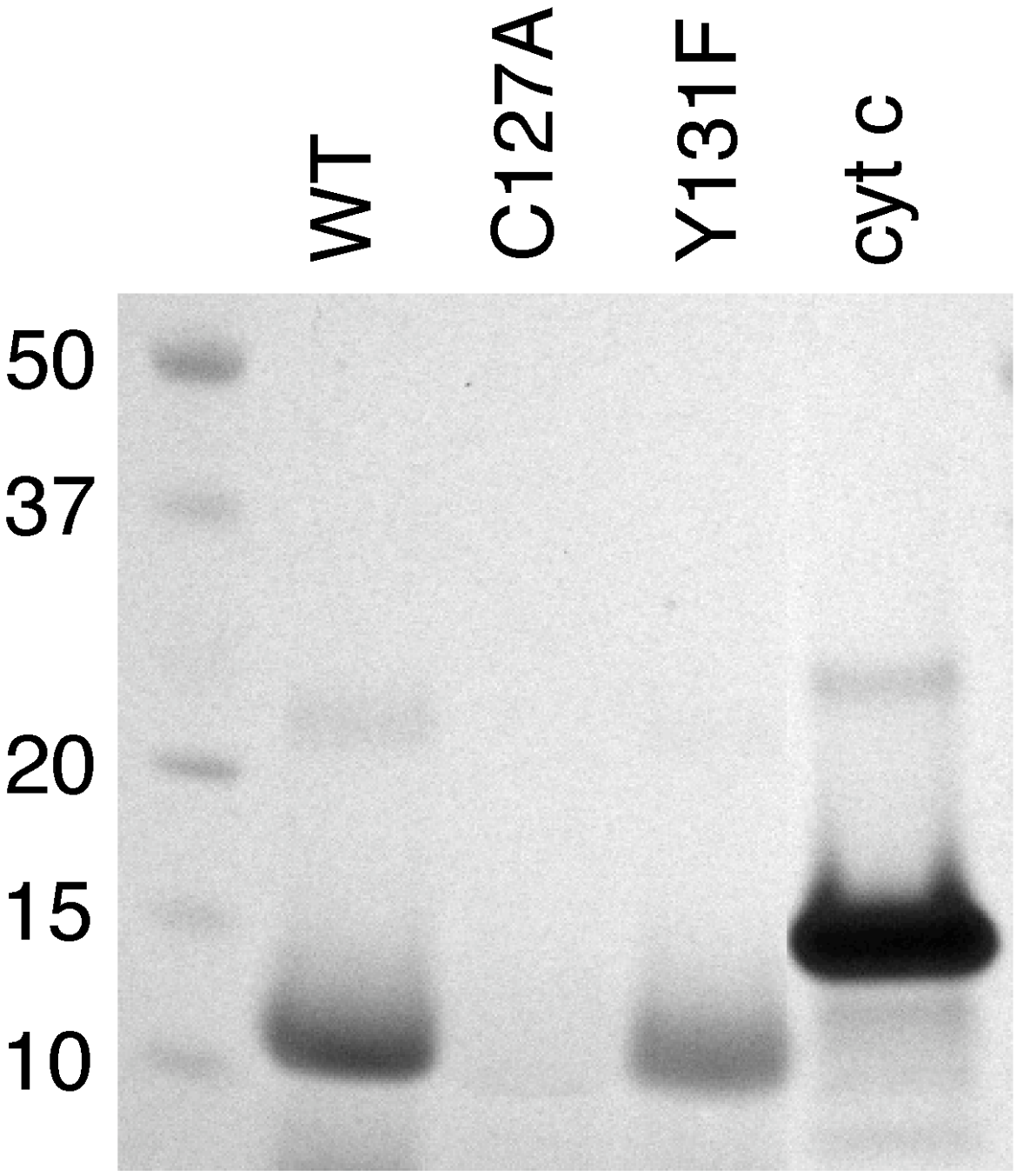

Figure S9. Heme-stained SDS-PAGE assay for ferric heme binding to wild type dvCcmE′, [C127A]-dvCcmE′, [Y131F]-dvCcmE′, and equine heart holocytochrome *c* (control). Molecular weights (kDa) of the standards in the left lane are indicated.

Supplementary References

1. Huang, Y. J., and Montelione, G.T. DisMeta disorder prediction server. Rutgers University. http://www-nmr.cabm.rutgers.edu/bioinformatics/disorder/.
2. Jansson M., Li, Y.-C., Jendeberg, L., Anderson, S., Montelione, G. T., and Nilsson, B. (1996) High level production of uniformly ^{15}N- and ^{13}C-enriched fusion proteins in *Escherichia coli*. *J. Biomol. NMR 7*, 131-141.
3. Kapust, R. B., Tözsér, J., Fox, J. D., Anderson, D. E., Cherry, S., Copeland, T. D., and Waugh, D. S. (2001) Tobacco etch virus protease: mechanism of autolysis and rational design of stable mutants with wild-type catalytic proficiency. *Protein Eng. 14*, 993-1000.
4. Delaglio, F., Grzesiek, S., Vuister, G. W., Zhu, G., Pfeifer, J., and Bax, A. (1995) NMRPipe: a multidimensional spectral processing system based on UNIX pipes. *J. Biomol. NMR 6*, 277-293.
5. Goddard, T. D., and Kneller, D. G. SPARKY 3. University of California, San Francisco.
6. Moseley, H. N. B., Monleon, D., and Montelione, G.T. (2001) Automatic determination of protein backbone resonance assignments from triple resonance nuclear magnetic resonance data. *Methods Enzymol. 339*, 91-108.
7. Bahrami, A., Assadi, A. H., Markley, J. L., and Eghbalnia, H. R. (2009) Probabilistic interaction network of evidence algorithm and its application to complete labeling of peak lists from protein NMR spectroscopy. *PLoS Comput. Biol. 5*, e1000307.
8. Neri, D., Szyperski, T., Otting, G., Senn, H., and Wüthrich K. (1989) Stereospecific nuclear magnetic resonance assignments of the methyl groups of valine and leucine in the DNA-binding domain of the 434 repressor by biosynthetically directed fractional ^{13}C labeling. *Biochemistry 28*, 7510-7516.

9. Moseley, H. N. B., Sahota, G., and Montelione, G. T. (2004) Assignment validation software suite for the evaluation and presentation of protein resonance assignment data. *J. Biomol. NMR 28*, 341-355.

10. Vuister, G. W., and Bax, A. (1993) Quantitative *J* correlation: a new approach for measuring homonuclear three-bond $J(H^NH^\alpha)$ coupling constants in ^{15}N-enriched proteins. *J. Am. Chem. Soc. 115*, 7772-7777.

11. Farrow N. A., Muhandiram, R., Singer A. U., Pascal, S. M., Kay, C. M., Gish, G., Shoelson, S. E., Pawson, T., Forman-Kay J. D., and Kay, L. E. (1994) Backbone dynamics of a free and phosphopeptide-complexed Src homology 2 domain studied by ^{15}N NMR relaxation. *Biochemistry 33*, 5984-6003.

12. Rückert, M., and Otting, G. (2000) Alignment of biological macromolecules in novel nonionic liquid crystalline media for NMR experiments. *J. Am. Chem. Soc. 122*, 7793-7797.

13. Kontaxis, G., Clore, G. M., and Bax, A. (2000) Evaluation of cross-correlation effects and measurement of one-bond couplings in proteins with short transverse relaxation times. *J. Magn. Reson. 143*, 184-196.

14. Güntert, P., Mumenthaler, C., and Wüthrich, K. (1997) Torsion angle dynamics for NMR structure calculation with the new program DYANA. *J. Mol. Biol. 273*, 283-298.

15. Herrmann, T., Güntert, P., and Wüthrich, K. (2002) Protein NMR structure determination with automated NOE assignment using the new software CANDID and the torsion angle dynamics algorithm DYANA. *J. Mol. Biol. 319*, 209-227.

16. Pascal, S. M., Muhandiram, D. R., Yamazaki, T., Forman-Kay, J. D., and Kay, L. E. (1994) Simultaneous acquisition of ^{15}N- and ^{13}C-edited NOE spectra of proteins dissolved in H_2O. *J. Magn. Reson. Ser. B 103*, 197-201.

17. Cornilescu, G., Delaglio, F., and Bax, A. (1999) Protein backbone angle restraints from searching a database for chemical shift and sequence homology. *J. Biomol. NMR 13*, 289-302.

18. Brünger, A. T., Adams, P. D., Clore, G. M., DeLano, W. L., Gros, P., Grosse-Kunstleve, R. W., Jiang, J.-S., Kuszewski, J., Nilges, M., Pannu, N. S., Read, R. J., Rice, L. M., Simonson, T., and Warren, G. L. (1998) Crystallography & NMR system: a new software suite for macromolecular structure determination. *Acta Crystallogr. D54*, 905-921.

19. Linge, J. P., Williams, M. A., Spronk, C. A. E. M., Bonvin, A. M. J. J., and Nilges, M. (2003) Refinement of protein structures in explicit solvent. *Proteins 50*, 496-506.

20. Lüthy, R., Bowie, J. U., and Eisenberg, D. (1992) Assessment of protein models with three-dimensional profiles. *Nature 356*, 83-85.

21. Sippl, M. J. (1993) Recognition of errors in three-dimensional structures of proteins. *Proteins 17*, 355-362.

22. Laskowski, R. A., MacArthur, M. W., Moss, D. S., and Thornton, J. M. (1993) PROCHECK: a program to check the stereochemical quality of protein structures. *J. Appl. Crystallogr. 26*, 283-291.

23. Lovell, S. C., Davis, I. W., Arendall III, W. B., de Bakker, P. I. W., Word, J. M., Prisant, M. G., Richardson, J. S., and Richardson, D. C. (2003) Structure validation by Cα geometry: ϕ, ψ, and Cβ deviation. *Proteins 50*, 437-450.

24. Davis, I. W., Leaver-Fay, A., Chen, V. B., Block, J. N., Kapral, G. J., Wang, X., Murray, L. W., Arendall III, W. B., Snoeyink, J., Richardson, J. S., and Richardson, D. C. (2007) MolProbity: all-atom contacts and structure validation for proteins and nucleic acids. *Nucleic Acids Res. 35*, W375-W383.

25. Bhattacharya, A., Tejero, R., and Montelione, G. T. (2007) Evaluating protein structures determined by structural genomics consortia. *Proteins 66*, 778-795.

26. Huang, Y. J., Powers, R., and Montelione, G.T. (2005) Protein NMR Recall, Precision, and F-measure scores (RPF scores): structure quality assessment measures based on information retrieval statistics. *J. Am. Chem. Soc. 127*, 1665-1674.

27. Zweckstetter, M. (2008) NMR: prediction of molecular alignment from structure using the PALES software. *Nat. Protoc. 3*, 679-690.

28. Shindyalov, I. N., and Bourne P. E. (1998) Protein structure alignment by incremental combinatorial extension (CE) of the optimal path. *Protein Eng. 11*, 739-747.

29. Ashkenazy, H., Erez, E., Martz, E., Pupko, T., and Ben-Tal, N. (2010) ConSurf 2010: calculating evolutionary conservation in sequence and structure of proteins and nucleic acids. *Nucleic Acids Res. 38*, W529-W533.

30. DeLano, W. L. The PyMOL Molecular Graphics System, Version 1.1, Schrödinger LLC, http://www.pymol.org.

31. Palmer III, A. G., Rance, M., and Wright, P. E. (1991) Intramolecular motions of a zinc finger DNA-binding domain from Xfin characterized by proton-detected natural abundance ^{13}C heteronuclear NMR spectroscopy. *J. Am. Chem. Soc. 113*, 4371-4380.

32. Mandel, A. M., Akke, M., and Palmer III, A. G. (1995) Backbone dynamics of *Escherichia coli* ribonuclease HI: correlations with structure and function in an active enzyme. *J. Mol. Biol. 246*, 144-163.

33. Cole, R., and Loria, J. P. (2003) FAST-Modelfree: a program for rapid automated analysis of solution NMR spin-relaxation data. *J. Biomol. NMR 26*, 203-213.

34. Shack, J., and Clark, W. M. (1947) Metalloporphyrins. VI: Cycles of changes in systems containing heme. *J. Biol. Chem. 171*, 143-187.

35. Thomas, P. E., Ryan, D., and Levin, W. (1976) An improved staining procedure for the detection of the peroxidase activity of cytochrome *P*-450 on sodium dodecyl sulfate polyacrylamide gels. *Anal. Biochem. 75*, 168-176.

36. Berry, E. A, and Trumpower, B. L. (1987) Simultaneous determination of hemes *a*, *b*, and *c* from pyridine hemochrome spectra. *Anal. Biochem. 161*, 1-15.

37. Kay, L. E., Torchia, D. A., and Bax, A. (1989) Backbone dynamics of proteins as studied by ^{15}N inverse detected heteronuclear NMR spectroscopy: application to staphylococcal nuclease. *Biochemistry 28*, 8972-8979.

38. Fushman D., Weisemann R., Thüring H., and Rüterjans H. (1994) Backbone dynamics of ribonuclease T1 and its complex with 2´-GMP studied by two-dimensional heteronuclear NMR spectroscopy. *J. Biomol. NMR 4*, 61-78.

39. Wishart, D. S., and Sykes, B. D. (1994) The ^{13}C chemical-shift index: a simple method for the identification of protein secondary structure using ^{13}C chemical-shift data. *J. Biomol. NMR 4*, 171-180.

40. Enggist, E., Thöny-Meyer, L., Güntert, P., and Pervushin, K. (2002) NMR structure of the heme chaperone CcmE reveals a novel functional motif. *Structure 10*, 1551-1557.